IEEE TRANSACTIONS ON ELECTRON DEVICES

# Close-Packed PEDOT:PSS-Coated Graphene

# Microelectrodes for High-Resolution Interrogation of Neural Activity

Feng Sun, *Graduate Student Member, IEEE*, Zheshun Xiong, Jinyoung Park, and Guangyu Xu<sup>®</sup>, *Member, IEEE* 

Abstract — Graphene microelectrode arrays (MEAs) have emerged as a viable neurointerfacing tool for their combined benefits in mechanical, electrical, and optical properties. To evaluate their promise for high-resolution neurointerfacing applications, here we presented a 28- $\mu$ m pitched, poly (3, 4-ethylenedioxythiophene) polystyrene sulfonate (PEDOT:PSS)-coated graphene MEA that can achieve one order higher spatial resolution than previous graphene MEAs in both neurostimulation and optogenetic electrophysiology. The electroplated PEDOT:PSS layer improved the impedance and the charge-injection capacity of the graphene electrodes by 40-60 times (sub-100 k $\Omega$ , >1.31 mC/cm<sup>2</sup>) and maintained low light-induced artifacts among them (sub-3  $\mu$ V). As a result, our MEA was able to stimulate neuronal ensemble with single electrodes and record optogenetically evoked neural spikes with high signal-to-noise ratios. These results shed light on the possible use of PEDOT:PSS-coated graphene MEAs toward highresolution interrogation of neural activity.

Index Terms—Graphene microelectrodes, highresolution neurointerfacing, neurostimulation, optogenetic electrophysiology, poly (3, 4-ethylenedioxythiophene) polystyrene sulfonate (PEDOT:PSS) electroplating.

# I. INTRODUCTION

**P**RECISE interrogation of neural activity is essential in understanding the heterogeneity of neural networks [1], which requires the advancement of high-resolution neurointerfacing tools. In this perspective, close-packed silicon-based microelectrodes have been recognized for their capability to record and stimulate neural activity with high spatiotemporal resolution [2]–[6]. When these electrodes were placed in a  $10-20~\mu m$  pitch, the typical size of single neurons, the resulting microelectrode array (MEA), would be able to interrogate neural activity down to cellular levels. For instance, the  $20-\mu m$  pitched silicon-based MEAs (i.e., neuropixels probes built by  $0.13-\mu m$  CMOS technology [2]) have been able to simultaneously record more than 700 individual neurons

Manuscript received February 10, 2021; revised April 1, 2021; accepted April 15, 2021. This work was supported by the National Science Foundation under Grant ECCS-1835268 and Grant ECCS-2046031. The review of this article was arranged by Editor M. Caironi. (Corresponding author: Guangyu Xu.)

The authors are with the Department of Electrical and Computer Engineering, University of Massachusetts at Amherst, Amherst, MA 01003 USA (e-mail: guangyux@ umass.edu).

Color versions of one or more figure in this article are available at https://doi.org/10.1109/TED.2021.3074353.

Digital Object Identifie 10.1109/TED.2021.3074353

from multiple brain regions in an awake mouse, where spatial oversampling the neurocircuitry can attribute recorded spiking events to individual neurons [2]. In another example, a 17.5- $\mu$ m pitched CMOS MEA has succeeded extracellular stimulation of individual neurons cultured *in vitro* in a dense population and suggested its promise in a variety of high-precision neuromodulation experiments [3], [4].

Over the past decade, graphene-based MEAs have been suggested as a viable alternative to the industry-standard silicon-based MEAs [7]-[14]. These graphene electrodes are recognized for their combined benefits in mechanical compliance [7]-[13], low impedance [11], [13], [14], biocompatibility [7]-[9], [11]-[13], high transparency [7]-[12], [14], and low light-induced artifact [7], [10]-[12]; the latter two lend themselves to co-work with neuroimaging and optogenetic electrophysiology, which is challenging to achieve using silicon-based MEAs. For these reasons, graphene-based MEAs have been built on flexible substrates to reduce the tissue damage [7]-[12] and applied for in vivo neurointerfacing with simultaneous Ca<sup>2+</sup> imaging [7], [9], [11], [12] or optogenetic experiments [8], [12]. To date, such MEAs based on monolayer or four-layer graphene have been applied for neurostimulation [9], [13] and optogenetic electrophysiology [8], [10], [12]. The former is essential to form graphene-MEA based closed-loop neurointerfacing, whereas the latter allows for electrophysiology studies under cell-type specific, temporally precise optogenetic control. However, these arrays were typically built in a 300–900- $\mu$ m pitch [7]–[13], which cannot interrogate neural activity down to cellular levels as silicon-based MEAs do.

To record and control neural activity at high spatial resolutions, these graphene electrodes need to be further engineered (e.g., via surface coating [11], [14]) to feature low impedance (for low-noise recording [15]), low light-induced artifact (to co-work with neuroimaging and optogenetic electrophysiology [10]), and high charge injection capacity (CIC, for neurostimulation [9], [13], [15]) at small sizes [16]. In this perspective, graphene electrodes coated with Pt nanoparticles [11] and a PEDOT:PSS layer [14], [16] have been recently noted for their low impedance due to the increase of their effective surface area [16]–[19]; the latter have also shown low light-induced artifact during the optogenetic electrophysiology experiments in embryonic kidney cells [16]. Nonetheless, there have been limited experimental efforts to examine if these

0018-9383 © 2021 IEEE. Personal use is permitted, but republication/redistribution requires IEEE permission. See https://www.ieee.org/publications/rights/index.html for more information.

surface-coated graphene electrodes can form high-density MEAs that can interrogate neural activity ideally down to cellular levels.

To this end, here we report a 28-μm pitched PEDOT:PSScoated graphene MEA that features high yield (100%), low-impedance (sub-100 k $\Omega$ ), low light-induced artifact (sub-3  $\mu$ V), and high CIC (>1.31 mC/cm<sup>2</sup>). As a result, our MEA achieved one order higher spatial resolution than previous graphene MEAs in both neurostimulation and optogenetic electrophysiology experiments, enabled by the optoelectronic properties of the PEDOT:PSS layer coated on top of the bare graphene. In the former, we observed reliable Ca<sup>2+</sup> influx triggered by voltage pulses applied to individual electrodes, where the Ca<sup>2+</sup> signal decreases in neurons distance away from the stimulating electrodes. In the latter, our MEA can reliably record optogenetically stimulated neural spikes, whose amplitudes qualitatively match the neuron positions with respect to the recording electrodes. These results shed light on the possible use of PEDOT:PSS-coated graphene MEAs toward high-resolution interrogation of neural activity. Combined with its mechanical compliance and scalable fabrication steps, our PEDOT:PSS-coated graphene MEA may be ultimately built onto flexible substrates for in vivo use [7]-[13], or integrated to micron-sized light-emission-diode (µLED) arrays for closedloop neurointerfacing [10], [20]

#### II. METHODS

# A. Array Fabrication and Characterization

Our graphene MEA was based on chemical-vapordeposition (CVD) grown 3-5 layered graphene electroplated with a PEDOT:PSS layer as we reported before [16]. Using NR9/LOR-based bilayer lithography (with LOR being the sacrificial layer on the bottom), we patterned graphene electrodes in a 28-µm pitch by O<sub>2</sub>-plasma RIE step. We then dipped the chip into acetone to remove the NR9, but purposely left the LOR layer on top of the graphene, which served to protect graphene from being damaged during the following steps. These patterned electrodes were then contacted by Ti/Au layers (7/80-nm wires and 10/150-nm pads), and passivated by a 4- $\mu$ m-thick SU8 layer with 21  $\mu$ m × 10  $\mu$ m sized opening that defined the electrode area. The SU8 layer was later treated by O<sub>2</sub>-plasma to enhance its hydrophilicity [16] (graphene being protected by photoresist). Finally, the LOR layer was removed by a tetramethylammonium hydroxide-based developer.

We next wire-bonded the passivated MEA onto a printed circuit board (PCB) and encapsulated it with thermally cured polydimethylsiloxane (PDMS) layers. The packaged device was then configured in a three-electrode setting [Fig. 1(a)]—using Reference 600+ for both the PEDOT:PSS electroplating step and electrochemical characterizations of the MEA.

Specifically, for array electrochemical characterization, we conducted electrochemical impedance spectroscopy (EIS, 0.1--100 kHz, 10--mV rms ac excitation), cyclic voltammetry (CV, ten cycles from -0.6 to 0.8 V at 1000 mV/s scan rate), and voltage transient (VT, biphasic current pulses with  $500\text{-}\mu\text{s}$  duration) measurements using the three-electrode configuration. The MEA was placed inside a home-built Faraday cage,

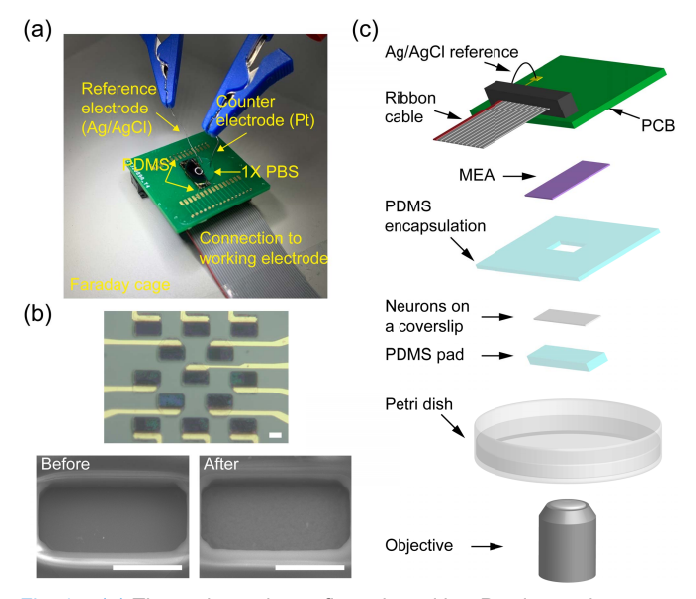


Fig. 1. (a) Three-electrode configu ation with a Pt wire as the counter electrode and an Ag/AgCl wire as the reference electrode. The working electrode (graphene) is accessed to Gamry 600+ via a ribbon cable. The Faraday cage was connected to the earth ground during the electrochemical characterizations. (b) Optical image of a PEDOT:PSS-coated graphene MEA (top) and representative SEM images of the graphene electrodes before (bottom left) and after (bottom right) PEDOT:PSS coating. Scale bar, 10  $\mu m$ . (c) Schematic view of the neurointerfacing setup.

immersed in  $1 \times PBS$  solution, and configured by Gamry Reference 600+ in the potentiostat mode [Fig. 1(a)].

To electroplate PEDOT:PSS on individual graphene electrodes, we used the same method as we reported before [16]. Briefly, we injected 2.1 mA/cm² current from the select graphene electrode for ca. 10 s in an aqueous mixture of 1% poly(sodium-p-styrenesulfonate) (PSS, 70 000 g/mol, ACROS Organics) and 0.02 mol/L (EDOT, 97%, Sigma-Aldrich). We then applied an additional 10 s electroplating step to all electrodes to lower electrode-to-electrode variation. After that, the resulting electrodes featured similar EIS impedance across the array (see Section III), although some of them exhibited nonuniformity in their electroplated PEDOT:PSS layer [Fig. 1(b)]. The resulting array was characterized again before additional neuron experiments.

### B. Cell Seeding and Transfection

Primary rat cortex neurons (Thermofisher) were cultured according to the official protocols. Specifically, we first sterilized coverslips by immersing them in 30% HCl for 1 h and acetone/isopropyl alcohol for 10 min, respectively. After autoclaving, we immediately placed the sterilized coverslips in 48-well plates and coated them with Poly-D-Lysine (50  $\mu$ g/ml, ThermoFisher) for 1 h at room temperature to improve cell adhesion. Primary rat cortex neurons were then seeded on the sterilized coverslips (placed in well plats) with the complete Neurobasal Plus Medium (Thermofisher) and incubated at 37 °C with 5% CO<sub>2</sub>.

After 96 h of neuron seeding, we transfected neurons with  $Ca^{2+}$  reporters (*GCaMP7s* [21], Addgene) or red-shifted opsins (*Chrimson* [22], Addgene) by adding 5  $\mu$ L ready-to-use AAV-viral preparation solution to each well. The transfected

neurons were incubated until full expression of *GCaMP7s* (120 h after transfection) or *Chrimson* (36 h after transfection) before further neuromodulation or optogenetic electrophysiology experiment, respectively.

#### C. Neurointerfacing Experiments

To prepare for the neurointerfacing experiments with our PEDOT:PSS-coated MEA, we applied an experimental setup based on inverted fluorescence microscopy as we reported before [16] [Fig. 1(c)], which served to provide Ca<sup>2+</sup> imaging capability and optogenetic stimulus to identify the MEAstimulated cells and conduct optogenetic electrophysiology, respectively. Briefly, we side-flipped the PCB with the encapsulated MEA and packaged it (via PDMS) onto a home-built lifting station with a manual lab jack. An Ag/AgCl wire was soldered to the backside of the PCB to later act as the pseudo-reference electrode. We then transferred the coverslip seeded with neurons to the PDMS pad mounted on a Petri dish, which was filled with an imaging solution containing 145-mM NaCl, 2.5-mM KCl, 10-mM glucose, 10-mM HEPES, pH 7.4, 2-mM CaCl<sub>2</sub>, and 1-mM MgCl<sub>2</sub> [23]. The Petri dish was then placed on the stage of an epifluorescence inverted microscope (Leica) equipped with a K5 scientific CMOS camera and a pE-4000 light source (CoolLED). This microscope served to identify and confirm the optogenetically responsive cells by GCaMP7s imaging and to deliver the optogenetic stimulus for Chrimson-expressed neurons. The flip-sided MEA (wirebonded on PCB) was then lowered, aligned to, and contacted with targeted neurons by fine-tuning the lifting station, with the cell imaging medium being biased by the Ag/AgCl.

For neuromodulation experiment, we applied 1, 3, and 4 trains of biphasic voltage pulses ( $\pm 0.5$  V) to the selected graphene electrode by an A-M Model 4100 stimulator, which was synchronized with the camera using Leica Application Suite X software. Simultaneously, GCaMP7s-expressed neurons were imaged at 2 frame/s (100-ms exposure time per frame, no binning) with a PL Fluotar  $20\times$  objective lens (NA = 0.4, Leica) at room temperature, using 2.21 mW/mm² 470/40-nm excitation pulsed at 2 frame/s, a 495-nm long-pass dichroic mirror, and a 520/40-nm emission filter.

To conduct an optogenetic electrophysiology experiment, the MEA wire-bonded on PCB was then accessed by an electrophysiology amplifier chip (RHD2164, Intan Technologies) via a ribbon cable, which was triggered by the camera to synchronize the recording data with the camera of the microscope (served to offer 550/15-nm optogenetic stimulus). After making the MEA-neuron contact by finetuning the lifting station, the Ag/AgCl reference electrode was immersed into the cell imaging medium. The recording signals were sampled at 20-kHz and bandpass filtered at 100 Hz–3 kHz; the 60-Hz noise and dc offset were removed by built-in filters of an Intan RHD USB interface software (Intan Technologies).

#### III. RESULTS AND DISCUSSIONS

#### A. Electrochemical Characterization

We found that the electroplated PEDOT:PSS layer was effective in altering the EIS (from 0.1 to 100 kHz), CV

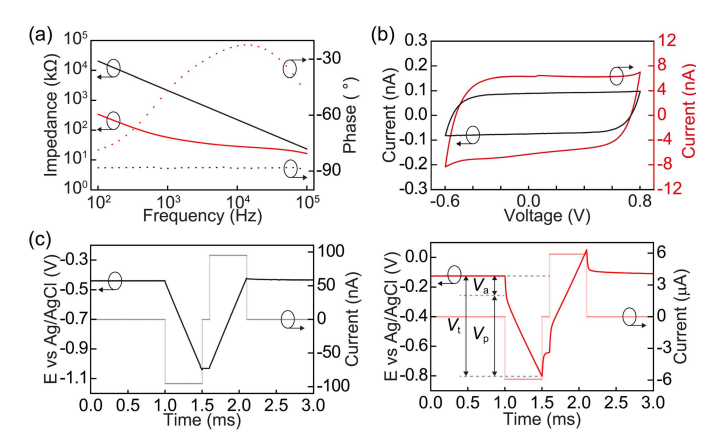


Fig. 2. Electrochemical characterization of a typical electrode before (black) and after PEDOT: PSS coating (red). (a) EIS impedance (solid line) and phase (dashed line). (b) CV measured in the tenth cycle and scanned at 1000 mV/s. (c) Voltage transients (dark) under a biphasic current pulse (light).  $V_{\rm p}, V_{\rm a}$ , and  $V_{\rm t}$  represent the negative polarization voltage, the access voltage, and the maximum voltage drop in the VT trace, respectively.

(from -0.6 to 0.8 V), and VT (biphasic current pulsing) data measured from the MEA. First, after the electroplating step, all 13 electrodes dropped their EIS impedance amplitude at 1 kHz from 2.10  $\pm$  0.80 M $\Omega$  to 54  $\pm$  9 k $\Omega$  and increased their EIS phase in the entire frequency range [Fig. 2(a)]. This result suggests that the PEDOT:PSS layer effectively reduced the electrode impedance, and changed the electrodes to be less capacitive (i.e., away from  $-90^{\circ}$  phase). Such 28- $\mu$ m-pitched, sub-100-k $\Omega$  electrodes are desired for a high signal-to-noise ratio (SNR) in high-density electrophysiology. Second, we measured a total of ten cycles of CV (scanned at a rate of 1000 mV/s) in five electrodes in the array (four at the corners and one at the center) and chose the data measured in the tenth cycle for analysis when it settled to the equilibrium [11] [Fig. 2(b)]. Our data show that the PEDOT:PSS electroplating step increased the current values in the CV curves by ca. one order with no apparent redox peaks. This result suggests that the PEDOT:PSS layer increased the amount of non-Faradaic charging processes [24], [25], likely because its roughness and porosity effectively increased the surface area of the electrode, and thus decreased the electrode impedance by lowering the charge transfer resistance and increasing the double layer capacitance [10], [17], [18], [26], [27]. Third, our VT data in Fig. 2(c) show that the PEDOT:PSS layer increased the maximum injection current when the negative polarization voltage  $(V_p)$  did not go beyond the water window (chosen here as -0.6 V for PEDOT:PSS-coated electrodes [18]) by ca. 60 times [9], [28]–[31]. Here,  $V_p$  was calculated by subtracting the access voltage ( $V_a$ , the voltage drop 10  $\mu$ s after applying the cathodic current pulse) from the maximum voltage drop in the trace  $(V_t)$ . Such increase is likely because the PEDOT:PSS layer (estimated to be ca. 270 nm thick according to the density of transferred charges by the end of the electroplating steps [32]) lowered the charge transfer resistance and thus facilitated the charge injection process. As a result, the charge injection capacity (CIC, defined in [15])

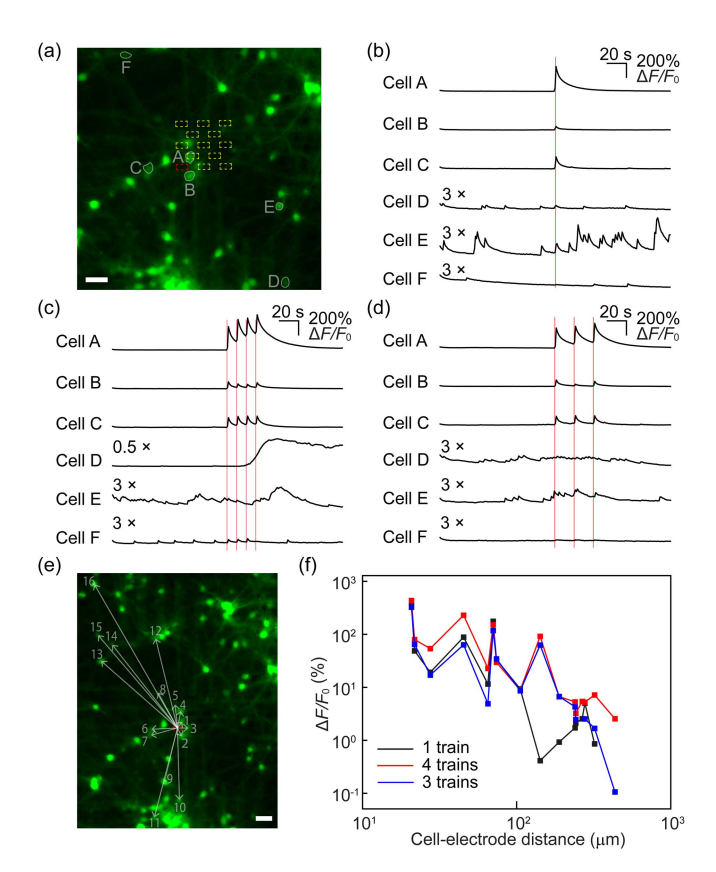


Fig. 3. Neurostimulation experiment. (a) *GCaMP7s* image of neurons contacted with the MEA. A total of 12 electrodes are marked in yellow; the stimulation electrode is marked in red. Scale bar, 40  $\mu m$ . (b)–(d)  $\Delta F/F_0$  traces in six representative neurons next to the stimulating electrode (cells A–F) under 1, 4, and 3 trains of biphasic voltage pulses, respectively. The number next to each trace is the scaling factor; each red line represents a train of biphasic voltage pulses (50 5–ms periods with  $t_{+0.5} V/t_{-0.5} V/t_{0V} = 0.5/0.5/4$  ms in each). (e) *GCaMP7s* image of 16 neurons that responded to all trains of voltage pulses we applied in (b)–(d). Neurons (pointed by arrows) are numbered with their center-to-center distance to the stimulating electrode (red). Scale bar, 40  $\mu m$ . (f)  $\Delta F/F_0$  versus cell-to-electrode distance under 1 (black), 4 (red), and 3 trains (blue) of biphasic voltage pulses.

values increased from 0.02 to 1.40 mC/cm<sup>2</sup>, which is desired to achieve effective neurostimulation [33].

#### B. Neuromodulation With Single Electrodes

We found a close MEA-cell contact (ca.  $10~\mu m$ , estimated by the precision of the focus adjustment in our microscope) is critical here to achieve effective electrical field stimulation of neurons since a long cell-electrode distance will significantly dampen the voltage drop evoked across the neuron membrane [34], [35]. After MEA-cell close contact, we then selected one single PEDOT:PSS-coated electrode next to the targeted responsive neurons (i.e., stimulating electrode) and applied trains of biphasic voltage pulses (each train has 50 5-ms periods with  $t_{+0.5} \text{V}/t_{-0.5} \text{V}/t_{0} \text{V} = 0.5/0.5/4$  ms in each) to electrically stimulate these neurons. Such voltage stimulation patterns were chosen to keep the voltage across the electrode–electrolyte interface within the water window and found to be more effective than current stimulation patterns in evoking neural spikes in our setup.

Specifically, we synchronized the Ca<sup>2+</sup> imaging data (i.e.,  $\Delta F/F_0$  traces via GCaMP7s) with 1-4 trains of the aforementioned biphasic voltage pulses and applied to the selected electrode [marked in red, see Fig. 3(a)]. The results show that these voltage pulses can reliably trigger Ca2+ influx in neurons next to the stimulating electrode [representative cells A-F in Fig. 3(b)-(d), evidenced by the transient increase in their  $\Delta F/F_0$  traces right after each train of voltage pulses,  $F_0$  is defined as the 5-s average right before we applied the first train of voltage pulses]. We observed that such electrodeevoked Ca<sup>2+</sup> transients often took a few seconds to settle back to the baseline (e.g., cells A-C, and F), which is consistent with prior works on intracellular Ca<sup>2+</sup> dynamics reported by GCaMP7s [21]. It is also noted that some neurons responded to the voltage pulses with multiple Ca<sup>2+</sup> spikes (e.g., cell E) or did not respond to all trains of voltage pulses (e.g., cells D-F in Fig. 3(c), likely due to details in their neighboring neurocircuitry (i.e., numbers/intensities of synapses nearby) or the cell-to-cell variation (i.e., heterogeneity among the cultured neurons). The fact that our 28-µm-pitched MEA can reliably evoke a neural response with single electrodes echoes the high CIC values in PEDOT:PSS-coated electrodes. Moreover, neurons remained healthy after neurostimulation experiments, evidenced by their shape and capability to fire natural spikes. As a result, our MEA can be one order denser than previous graphene MEAs used for neurostimulation, suggesting its promise for high-resolution neurointerfacing.

We next quantified the evoked neural spiking intensities (i.e., peak values of  $\Delta F/F_0$ ) among all 16 neurons in the field of view [Fig. 3(e)] that responded to all trains of voltage pulses we applied in Fig. 3(b)-(d) (cells D-F were not included). By measuring the center-to-center distance of these neurons to the stimulating electrode, we found that neurons being laterally closer to the stimulating electrode generally featured higher peak  $\Delta F/F_0$  values (with ca. second-order difference), albeit cell-to-cell variation may also come into play (Fig. 3(f), averaged from 1, 3, or 4 trains). Such decay of  $\Delta F/F_0$  values as the cell-electrode distance increases is likely because neurons further away from the stimulating electrode were evoked by an attenuated electrical field, whose intensity was weakened by the cell medium. This result suggests that our MEA can locally stimulate neurons close to the select stimulating electrode, which is desired for high-resolution neurostimulation.

## C. High-Fidelity Optogenetic Electrophysiology

To conduct optogenetic electrophysiology experiments, we need to examine whether our PEDOT:PSS-coated electrodes could feature *both* low impedance (for high signal-to-noise ratios, SNR) and low light-induced artifact (for high signal-to-background ratios, SBR), two equally important figures-of-merit to achieve high-fidelity recording [16]. To this end, we first quantified the light-induced artifact of our MEA using the same setup as the neurostimulation experiment but without neurons placed in the Petri dish. Specifically, we accessed the MEA with an Intan RHD2164 chip (synchronized with the microscope camera) and sampled the baseline signals with the electrodes being immersed in cell medium

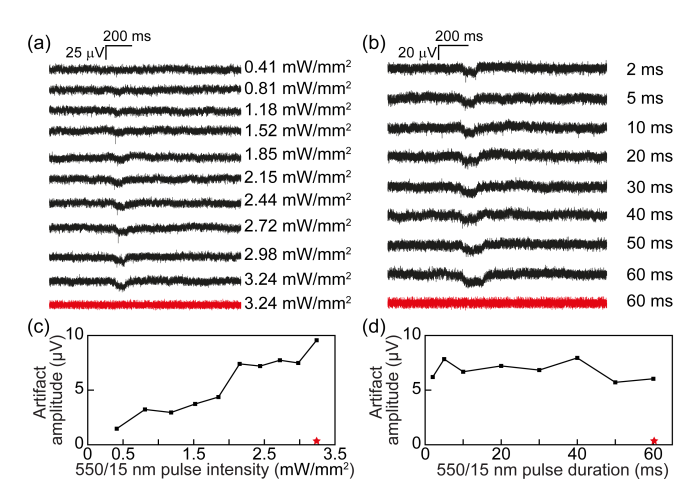


Fig. 4. Weak light-induced artifact. (a) Artifact traces (with no neurons) with a single 550/15-nm pulse (2-ms duration) at varying light intensities. (b) Artifact traces (with no neurons) with a single 550/15-nm pulse (3.24-mW/mm² intensity) at varying pulse durations. In (a) and (b), the red trace was recorded when one 100-Hz high pass filter is applied to the Intan chip. (c) Artifact amplitude versus light intensity at 2-ms duration. (d) Artifact amplitude versus light intensity at 3.24 mW/mm² intensity. In (c) and (d), the artifact amplitudes are define as the absolute values of the minimum in the 1000-point adjacent-averaged traces; the red stars represent the artifact amplitude when we applied the 100-Hz high-pass filter to the Intan chip.

(sampled at 20 kHz and bandpass filtered at 0.1 Hz-3 kHz). The recorded traces showed a sub-3- $\mu$ V root-mean-square (rms) noise level [7], suggesting that our low-impedance electrodes are suitable for low noise recording. We then illuminated the MEA with pulsed 550/15-nm optogenetic stimulus (using the inverted microscope) at varying light intensities and pulse durations (Fig. 4). Such optogenetic stimulus was found to result in a transient negative voltage in the recorded traces (i.e., light-induced artifact), likely due to the negatively charged counter-ions near the electrode [16]. The artifact amplitude, defined here as the amplitude of the minimum in the recorded traces, increased with the light intensity from 0.41 to 3.24 mW/mm<sup>2</sup> [ranging 5–10  $\mu$ V in Fig. 4(c)] but only weakly depended on the pulse duration from 2 to 100 ms [ca. 10  $\mu$ V in Fig. 4(d)], a trend similar to what has been reported in Au MEAs [10]. Importantly, we noted that these small light-induced artifacts were largely slow varying signals and can be filtered out by applying a 100-Hz high-pass filter to the sampled trace [see red traces in Fig. 4(a) and (b)]. For this reason, we chose to conduct optogenetic electrophysiology under 0.05-0.41 mW/mm<sup>2</sup> 550/15-nm stimulus, which was pulsed 1, 5, and 10 Hz with 2-ms duration (a condition reported in Chrimson-expressed neurons [22]); the data were then bandpass-filtered at 100 Hz-3 kHz to eliminate the light-induced artifacts.

We then conducted optogenetic electrophysiology on neurons expressed with *Chrimson*. With our low-impedance, low-artifact MEA, we were able to record multiple optogenetically evoked neural spikes after each 550/15-nm pulse (a total of 50 pulses in a 10-s window), in contrast with the control traces measured without neurons (Fig. 5). Most of these spikes were considered to result from the optogenetic

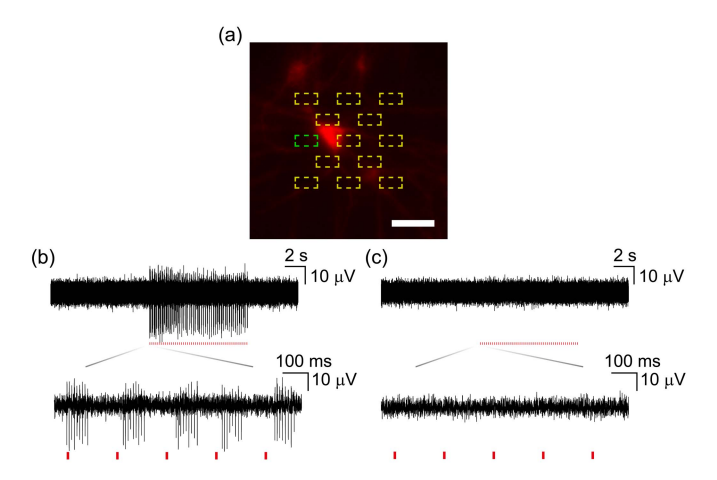


Fig. 5. Optogenetic electrophysiology experiments. (a) *Crimson* image of neurons contacted with the MEA. Electrodes are marked in dashed boxes; the central electrode (green) is selected for the following analysis. Scale bar, 40  $\mu$ m. (b) Five-point adjacent-averaging trace of the central electrode under 0.41 mW/mm² 550/15 nm optogenetic stimulus. (c) Control trace of the central electrode (measured without neurons) under 0.41 mW/mm² 550/15 nm optogenetic stimulus. In (b) and (c), the red stamps represent individual 550/15 nm pulses.

stimulus because we sparsely (if not none) recorded natural neural spikes outside the 10-s stimulus window. To quantify our electrophysiology data, we selected all recorded spikes whose negative amplitudes ( $V_{\text{neg}}$ ) were larger than five times the noise floor (measured in control traces), and performed spike-triggered-averaging [3], [6] by aligning their negative peaks [Fig. 6(a)]. The results show that: 1) the averaged peak-to-peak spike amplitudes,  $V_{\text{pp}}$ , were significant (ca. 30  $\mu$ V) compared to the spike-to-spike variation (<5  $\mu$ V) at all stimulus intensities (0.05–0.41 mW/mm²) and all pulsing frequencies (1–10 Hz), suggesting that our MEA can indeed achieve high-fidelity optogenetic electrophysiology and 2) the averaged spikes had ca. 1 ms duration, which is consistent with prior extracellular recording works [6].

Taking one step further, we found that the spike amplitude,  $V_{\rm pp}$ , was not strongly affected by the stimulus intensity and pulsing frequency, and the spiking frequency (i.e., the number of evoked spikes per 2-ms pulse) was. Specifically, our data showed that the spiking frequency increased with the stimulus intensity, but decreased with the pulsing frequency. These results suggest the following.

- Although the lowest stimulus intensity we applied, 0.05 mW/mm<sup>2</sup>, was sufficient to activate the *Chrimson* opsins expressed in neurons, stronger stimulus intensity was able to evoke more neural spiking events [Fig. 6(b)]. This is likely because more *Chrimson* channels were opened at a stronger stimulus, which may trigger multiple cycles of cation fluxes and thus the neural spiking [8].
- 2) Although *Chrimson* expressed neurons can respond to pulsing frequency up to 10 Hz, a higher pulsing frequency clearly reduced the spiking frequency from neurons. This phenomenon is likely due to the slow recovery kinetics of *Chrimson* channels [22], which may prevent

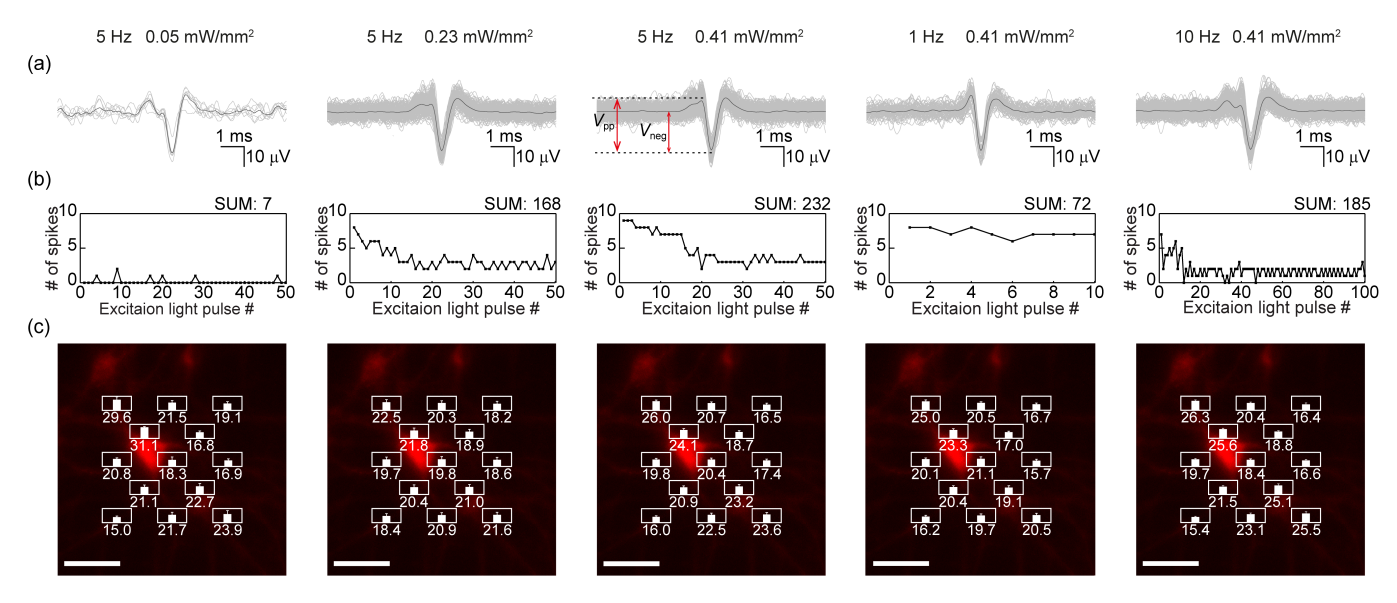


Fig. 6. Quantifica ion of the recorded neural spikes within the 10-s stimulus window under various stimulus intensities and pulsing frequencies. (a) Recorded spikes with their average shown in black. The spikes were selected for analysis if their negative spike amplitudes ( $V_{\text{neg}}$ ) were larger than fi e times the noise floo in control traces. (b) Number of evoked spikes per 550/15-nm pulse; the total number of selected spikes within the 10-s stimulus window is listed on the top (SUM). (c) Spatial mapping of  $V_{\text{neg}}$  [averaged by all selected spikes in (b)] across the MEA. A *Chrimson* image of neurons (contacted with the MEA) is overlaid with 13 electrodes indicated by white boxes. Bar plots in each box and the numbers on top indicate the  $V_{\text{neg}}$  amplitude each electrode has recorded. The height of each white box is 40  $\mu$ V. Scale bar, 40  $\mu$ m.

multiple cycles of cation fluxes between two neighboring 550/15-nm pulses.

We finally mapped the negative spike amplitudes,  $V_{\rm neg}$ , across the array, and compared it with the neuron positions to examine the spatial resolution of the MEA for optogenetic electrophysiology [Fig. 6(c)]. Our data showed that the  $V_{\rm neg}$  values were typically smaller among the electrodes further away from the targeted neurons, at all stimulus intensities and pulsing frequencies. This is as we expected since the electrodes away from the neuron may receive spiking signals that were attenuated in the cell medium. These results suggest that our MEA-collected data qualitatively match the position of optogenetically responsive neurons, which is desired for high-resolution optogenetic electrophysiology.

# IV. CONCLUSION

In sum, we presented a 28-µm-pitched PEDOT:PSS-coated graphene MEA that can achieve one order higher spatial resolution than prior graphene MEAs in both neurostimulation and optogenetic electrophysiology experiments. The electroplated PEDOT:PSS layer improved the EIS impedance and the CIC values by 40–60 times and maintained low light-induced artifacts. As a result, our MEA was able to stimulate neuronal ensemble with single electrodes (evidenced by Ca<sup>2+</sup> imaging) and record optogenetically evoked neural spikes with high SNRs. These results suggest the promise of PEDOT:PSScoated graphene MEA toward high-resolution interrogation of neural activity. Moving forward, we expect that these PEDOT:PSS-coated graphene electrodes can be further cooptimized for their optical transparency and electrochemical properties, fabricated onto the flexible substrate (e.g., Parylene C) for in vivo use, or integrated to micron-sized LED arrays for closed-loop neurointerfacing.

#### REFERENCES

- J. G. Nicholls, A. R. Martin, B. G. Wallace, and P. A. Fuchs, From Neuron to Brain, vol. 271. Sunderland, MA, USA: Sinauer Associates, 2001.
- [2] J. J. Jun et al., "Fully integrated silicon probes for high-density recording of neural activity," *Nature*, vol. 551, no. 7679, pp. 232–236, Nov. 2017, doi: 10.1038/nature24636.
- [3] J. Müller et al., "High-resolution CMOS MEA platform to study neurons at subcellular, cellular, and network levels," *Lab Chip*, vol. 15, no. 13, pp. 2767–2780, 2015, doi: 10.1039/c5lc00133a.
- [4] S. Ronchi et al., "Single-cell electrical stimulation using CMOS-based high-density microelectrode arrays," Frontiers Neurosci., vol. 13, p. 208, Mar. 2019, doi: 10.3389/fnins.2019.00208.
- [5] C. Xie, Z. Lin, L. Hanson, Y. Cui, and B. Cui, "Intracellular recording of action potentials by nanopillar electroporation," *Nature Nanotechnol.*, vol. 7, no. 3, pp. 185–190, Feb. 2012, doi: 10.1038/nnano.2012.8.
- [6] J. Abbott et al., "Extracellular recording of direct synaptic signals with a CMOS-nanoelectrode array," Lab Chip, vol. 20, no. 17, pp. 3239–3248, Aug. 2020, doi: 10.1039/D0LC00553C.
- [7] D. Kuzum et al., "Transparent and flexible low noise graphene electrodes for simultaneous electrophysiology and neuroimaging," Nature Commun., vol. 5, no. 1, pp. 1–10, Dec. 2014, doi: 10.1038/ ncomms6259.
- [8] D.-W. Park et al., "Graphene-based carbon-layered electrode array technology for neural imaging and optogenetic applications," Nature Commun., vol. 5, no. 1, pp. 1–11, Dec. 2014, doi: 10.1038/ ncomms6258.
- [9] D.-W. Park et al., "Electrical neural stimulation and simultaneous in vivo monitoring with transparent graphene electrode arrays implanted in GCaMP6f mice," ACS Nano, vol. 12, no. 1, pp. 148–157, Jan. 2018, doi: 10.1021/acsnano.7b04321.
- [10] X. Liu, Y. Lu, E. Iseri, Y. Shi, and D. Kuzum, "A compact closed-loop optogenetics system based on artifact-free transparent graphene electrodes," *Frontiers Neurosci.*, vol. 12, pp. 1–13, Mar. 2018, doi: 10.3389/ fnins.2018.00132.
- [11] Y. Lu et al., "Ultralow impedance graphene microelectrodes with high optical transparency for simultaneous deep two-photon imaging in transgenic mice," Adv. Funct. Mater., vol. 28, no. 31, Aug. 2018, Art. no. 1800002.
- [12] M. Thunemann et al., "Deep 2-photon imaging and artifact-free optogenetics through transparent graphene microelectrode arrays," Nature Commun., vol. 9, no. 1, pp. 1–12, Dec. 2018, doi: 10.1038/s41467-018-04457-5.

- [13] Y. Lu, H. Lyu, A. G. Richardson, T. H. Lucas, and D. Kuzum, "Flexible neural electrode array based-on porous graphene for cortical microstimulation and sensing," *Sci. Rep.*, vol. 6, no. 1, Dec. 2016, Art. no. 33526, doi: 10.1038/srep33526.
- [14] P. Kshirsagar et al., "Transparent graphene/PEDOT: PSS microelectrodes for electro- and optophysiology," Adv. Mater. Tech., vol. 4, no. 1, Jan. 2019, Art. no. 1800318, doi: 10.1002/admt.201800318.
- [15] S. F. Cogan, "Neural stimulation and recording electrodes," Annu. Rev. Biomed. Eng., vol. 10, no. 1, pp. 275–309, Aug. 2008, doi: 10.1146/annurev.bioeng.10.061807.160518.
- [16] J. Park, F. Sun, Y. Xie, Z. Xiong, and G. Xu, "Low-impedance low-artifact PEDOT: PSS-coated graphene electrodes towards high density optogenetic electrophysiology," *IEEE Electron Device Lett.*, vol. 41, no. 8, pp. 1261–1264, Aug. 2020, doi: 10.1109/LED.2020.3004126.
- [17] X. T. Cui and D. D. Zhou, "Poly (3,4-Ethylenedioxythiophene) for chronic neural stimulation," *IEEE Trans. Neural Syst. Rehabil. Eng.*, vol. 15, no. 4, pp. 502–508, Dec. 2007, doi: 10.1109/tnsre.2007.909811.
- vol. 15, no. 4, pp. 502–508, Dec. 2007, doi: 10.1109/tnsre.2007.909811.
  [18] Y. Qiang *et al.*, "Bilayer nanomesh structures for transparent recording and stimulating microelectrodes," *Adv. Funct. Mater.*, vol. 27, no. 48, pp. 1–11, 2017, doi: 10.1002/adfm.201704117.
- [19] D. Khodagholy et al., "NeuroGrid: Recording action potentials from the surface of the brain," *Nature Neurosci.*, vol. 18, no. 2, pp. 310–315, Feb. 2015, doi: 10.1038/nn.3905.
- [20] D. Mao, N. Li, Z. Xiong, Y. Sun, and G. Xu, "Single-cell opto-genetic control of calcium signaling with a high-density micro-LED array," iScience, vol. 21, pp. 403–412, Nov. 2019, doi: 10.1016/j.isci. 2019.10.024.
- [21] H. Dana et al., "High-performance calcium sensors for imaging activity in neuronal populations and microcompartments," *Nature Methods*, vol. 16, no. 7, pp. 649–657, Jul. 2019, doi: 10.1038/s41592-019-0435-6.
- [22] N. C. Klapoetke *et al.*, "Independent optical excitation of distinct neural populations," *Nature Methods*, vol. 11, no. 3, pp. 338–346, Mar. 2014, doi: 10.1038/nmeth.2836.
- [23] T.-W. Chen et al., "Ultrasensitive fluorescent proteins for imaging neuronal activity," Nature, vol. 499, no. 7458, pp. 295–300, Jul. 2013, doi: 10.1038/nature12354.
- [24] D. R. Merrill, M. Bikson, and J. G. R. Jefferys, "Electrical stimulation of excitable tissue: Design of efficacious and safe protocols," *J. Neurosci. Methods*, vol. 141, no. 2, pp. 171–198, Feb. 2005, doi: 10.1016/j. jneumeth.2004.10.020.

- [25] A. J. Bard and L. R. Faulkner, Electrochemical Methods: Fundamentals and Applications, 2nd ed. Hoboken, NJ, USA: Wiley, 2001, doi: 10.1023/A:1021637209564.
- [26] A. Elschner, S. Kirchmeyer, W. Lovenich, U. Merker, and K. Reuter, PEDOT: Principles and Applications of an Intrinsically Conductive Polymer. Boca Raton, FL, USA: CRC Press, 2010, doi: 10.1201/ b10318
- [27] J. Rivnay, H. Wang, L. Fenno, K. Deisseroth, and G. G. Malliaras, "Next-generation probes, particles, and proteins for neural interfacing," *Sci. Adv.*, vol. 3, no. 6, pp. 1–20, Jun. 2017, doi: 10.1126/sciadv. 1601649.
- [28] K. Wang et al., "High-performance graphene-fiber-based neural recording microelectrodes," Adv. Mater., vol. 31, no. 15, 2019, Art. no. 1805867.
- [29] V. Saunier, E. Flahaut, M.-C. Blatché, C. Bergaud, and A. Maziz, "Microelectrodes from PEDOT-carbon nanofiber composite for high performance neural recording, stimulation and neurochemical sensing," *MethodsX*, vol. 7, Oct. 2020, Art. no. 101106.
- [30] E. K. Brunton et al., "In vivo comparison of the charge densities required to evoke motor responses using novel annular penetrating microelectrodes," Frontiers Neurosci., vol. 9, p. 265, May 2015.
- [31] C. Boehler, T. Stieglitz, and M. Asplund, "Nanostructured platinum grass enables superior impedance reduction for neural microelectrodes," *Biomaterials*, vol. 67, pp. 346–353, Oct. 2015.
- [32] R. Gerwig et al., "PEDOT-CNT composite microelectrodes for recording and electrostimulation applications: Fabrication, morphology, and electrical properties," Frontiers Neuroeng., vol. 5, p. 8, May 2012, doi: 10.3389/fneng.2012.00008.
- [33] S. F. Cogan, P. R. Troyk, J. Ehrlich, T. D. Plante, and D. E. Detlefsen, "Potential-biased, asymmetric waveforms for charge-injection with activated iridium oxide (AIROF) neural stimulation electrodes," *IEEE Trans. Biomed. Eng.*, vol. 53, no. 2, pp. 327–332, Feb. 2006, doi: 10. 1109/tbme.2005.862572.
- [34] D. V. Palanker et al., "Attracting retinal cells to electrodes for high-resolution stimulation," Proc. SPIE, vol. 5314, pp. 306–314, Jul. 2004, doi: 10.1117/12.529757.
- [35] J. Kwon et al., "Nanoelectrode-mediated single neuron activation," Nanoscale, vol. 12, no. 7, pp. 4709–4718, Feb. 2020, doi: 10.1039/ c9nr10559i.